Available online at www.sciencedirect.com

ScienceDirect

Procedia Structural Integrity 52 (2024) 1–11

Structural Integrity Procedia

www.elsevier.com/locate/procedia

Fracture, Damage and Structural Health Monitoring

Limits of applicability of LEFM: numerical investigation on the crack-tip-yielding in a hollow-cylindrical specimen

D. Amato[a], L. Federico[b], E. Armentani[c], R. Citarella[a]

[a]*Department of Industrial Engineering, University of Salerno, via Giovanni Paolo II, Fisciano 84084, Italy*
[b] *Italian Aerospace Research Centre (CIRA), 81043 Capua, Italy*
[c] *Department of Chemical, Materials and Production Engineering, University of Naples Federico II, NA, Naples, 80125, Italy*

Abstract

Even if most Fatigue Crack Growth analyses are performed within the frame of Linear-Elastic Fracture Mechanics (LEFM), in some practical cases the boundaries of applicability of LEFM can be exceeded. This study analyses a fatigue crack growth under complex stress state, in a hollow cylindrical specimen with initial semielliptical surface crack, for which the LEFM limits are exceeded. The stresses in the surrounding of the crack tip, obtained by means of an elastic-plastic FE-analysis, are used to calculate the size of the plastic region and its shape. The analysis shows how the plastic zone size turns out to be comparable in size with the residual ligament and therefore the LEFM boundaries are exceeded. This outcome explains the misalignment found between the crack growth rates simulated by LEFM and the corresponding experimental results.

Keywords: crack growth; mode-I; cylindrical specimens; tension-torsion; LEFM's limits; elastic-plastic analysis

1. Introduction

The study of fracture mechanics has increased significantly during the last century, as more and more engineering applications require fracture mechanics assessments. The majority of fatigue crack growth analyses, both analytical and numerical, are performed on the basis of Linear Elastic Fracture Mechanics (LEFM) theory. This formulation of the phenomena involved in the analysis of cracks is really powerful but presents some weaknesses especially when it comes to local plasticity at the crack tip. The LEFM formulation of the SIF assumes that in the area immediately close to the crack tip, the stress grows indefinitely, independently from K_I. This is a consequence of the elasticity model of the material. In a real material though, plastic deformations take place, limiting the maximum value for the stresses.

10.1016/j.prostr.2023.12.001

The analytical methods developed for the analysis of the crack-tip-yielding, known as Elastic-Plastic Fracture Mechanics (EPFM) methods, are very limited. Elastic-plastic numerical models, capable of replicating the stress-strain state in the vicinity of crack tip, seem to be the only option at engineers and researchers disposal to make predictions on the crack growth behaviour. The most used approach to tackle the problem of local plasticity at the crack tip has been the Finite Element Method (FEM) [1][5]. In general, the large computational burden, due to the high accuracy required in the region surrounding the crack front, is a strong limit to such simulations [6].

This research activity aims at showing the risks of non-considering the limits of applicability of LEFM. The investigation was performed on a hollow-cylindrical specimen made of Al-alloy B95AT (analogue to Al-alloy 7075). In a preliminary study [7], the comparison between the outcomes of experimental tests and numerical simulations was performed. The LEFM approach used to analyse the problem was not able to reproduce the same crack propagation observed experimentally. Therefore, within this study, the reasons for this mismatch are analysed.

2. Experimental Tension-Torsion Tests

The experimental campaign, reported in [7], aimed at characterizing the fracture behaviour of the aluminium alloy B95AT (analogue to 7075 aluminium) under different loading conditions. A special test rig, including an optical microscope, was adopted to detect the crack path in real-time. Furthermore, it was made use of a beach mark procedure to mark several positions of the crack front as it grows. For more information on the full equipment used to perform the fracture tests, the reader is referred to [7].

The fracture parameters C and m i.e., the coefficients of the Paris' law, obtained from the fatigue-crack-growth tests [7], together with the main mechanical properties, such as the modulus of elasticity E, the monotonic tensile yield stress σ_y, the nominal and true ultimate tensile strength σ_n and σ_u, the final elongation δ and the strain hardening exponent and coefficient n and α, are listed in Table 1.

Table 1: Mechanical properties of Al-alloy B95AT [7].

E $[GPa]$	σ_y $[MPa]$	σ_n $[MPa]$	σ_u $[MPa]$	δ [%]	n [−]	α [−]	C	m
78.596	518	653	775	14	10.37	1.46	$1.6413 \cdot 10^{-10}$	2.917

The tests reported in [7] were performed using a hollow-cylindrical specimen in which a semi-elliptical surface crack was inserted at mid-span orthogonally to the specimen axis. The geometry is shown in Fig. 1: main dimensions are the outer diameter, $D = 28\ mm$, of the propagation domain and the inner diameter, $d = 10\ mm$. At middle height, the semi-elliptical initial notch, having a depth of $h = 3\ mm$ and an aspect ratio $h/c = 0.3$, was generated by means of the electro-spark method. The cross-sectional view in Fig. 1 depicts the characteristic crack dimensions a, b and c for a generic propagated crack front: a and c account respectively for the crack depth and width onto the initial crack plane, whereas b measures the superficial propagation, i.e., the distance existing between the advancing break-through point and the initial one.

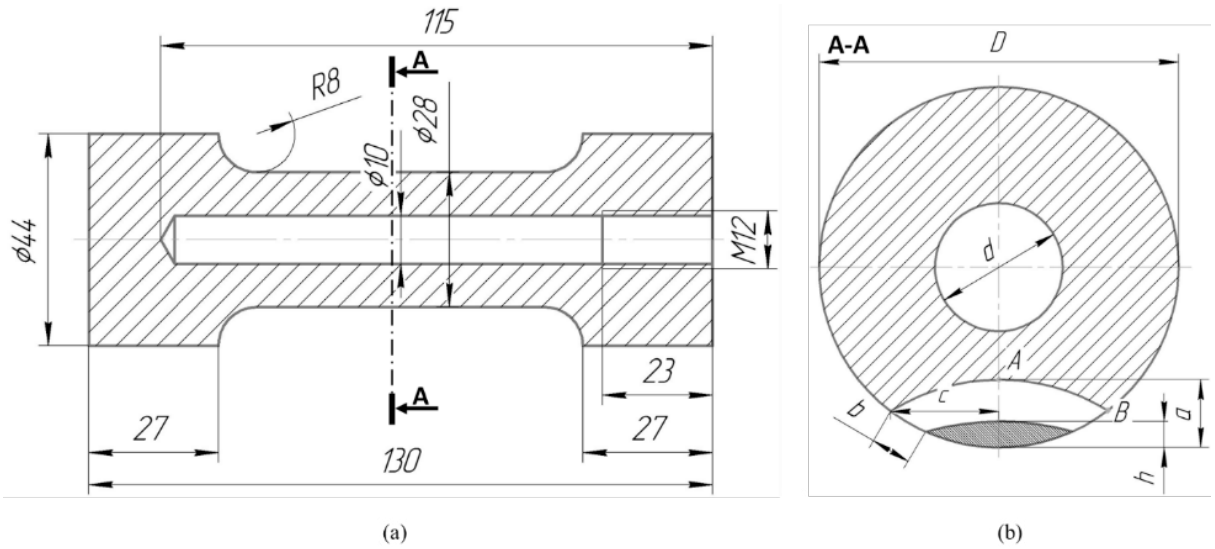

Fig. 1 (a) Hollow-Cylindrical specimen geometry; (b) cross-sectional view of initial elliptical notch [7].

The samples were tested in several loading conditions: cyclic tension, cyclic tension-torsion and pure cyclic torsion. The scope of this study is to analyse only the cyclic tension test as it showed a significant mismatch with the numerical simulation in terms of crack growth rates. In this test, the applied load was a cyclic axial force $F = 80\ kN$ with a stress ratio $R = 0.1$ and a frequency of $10\ Hz$.

3. Plasticity Models

Two stress-strain models were adopted to characterize the effective response of the material in the transition from the linear-elastic behaviour to the elastic-plastic one. The material is assumed to behave as elastic-plastic with isotropic hardening. The first inelastic analysis was performed using a Bi-Linear model (B-L), whereas a second attempt was performed with a non-linear stress-strain curve: the Ramber-Osgood stress-strain model (R-O-relationship). A comparison of the two material laws is provided in Fig. 2, where the difference between the two model is noticeable, especially in the transition area between the elastic and the plastic parts of the diagram.

3.1. Bi-Linear stress-strain model

The Bi-Linear stress strain model is a simple mathematical law used to approximate the complex elastic-plastic response of a metallic material undergoing a mechanical load. The idea behind this formulation is to assume a linear behaviour of the material across all its strength range. To discern between the elastic and the plastic region, two different material constants are defined: the Youngs or tangent modulus and the secant modulus, the latter defined as the slope of the line connecting the yield point with the ultimate tensile stress.

3.2. Ramber-Osgood (R-O) stress-strain model

The R-O relationship is a mathematical representation of the experimental stress-strain curve of a material. It approximately represents an estimation of the actual stress-strain relationship. The R-O theory states that the total strain is the sum of two separate terms: the elastic strain and the plastic one. The first follows a linear law with the stress whereas the plastic component of the strain is a power function of the stress. A common expression of the R-O relationship, as presented in [8], is:

$$\epsilon = \frac{\sigma}{E} + \alpha \frac{\sigma_y}{E} \left(\frac{\sigma}{\sigma_y} \right)^n \tag{1}$$

The parameters σ and ϵ represent the stress and total strain, respectively; the material properties are listed in Table *1*.

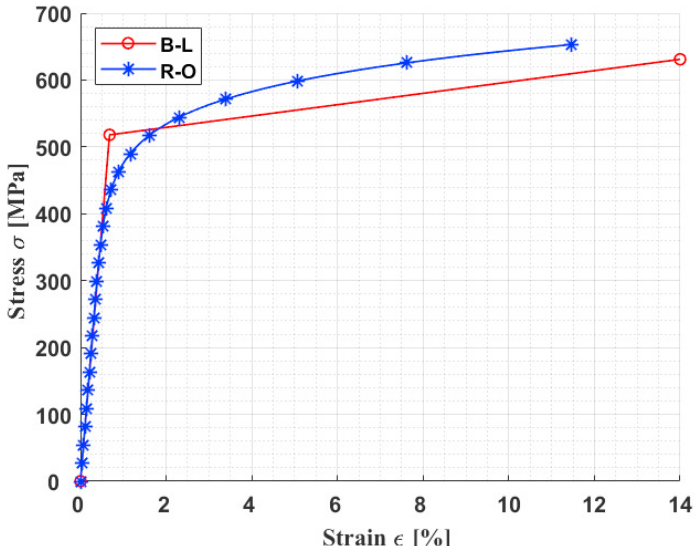

Fig. 2 Comparison of the two stress-strain model: Bi-Linear (B-L) and Ramber-Osgood (R-O).

In this study, the R-O law was chosen as it provides a smoother transition between the elastic and the plastic behaviour and it can simulate better the real response of the material.

4. Crack Growth Analyses

The aim of the analyses was to replicate the stage of the propagation during which the crack front approaches and intersects the axial hole of the specimen. In fact, at that stage of the propagation, the residual ligament between the crack front and the free surface of the hole is small compared with the dimension of the crack front plastic zone.
The testing conditions have been replicated through a numerical model of the cracked specimen. The simulation procedure was performed by means of the combined use of the commercial software ABAQUS and FRANC3D [9]9,10]. Hereinafter, the simulation procedure and the numerical model preparation is explained.

4.1. Simulation Procedure

With reference to Fig. 3 the first step to create the model is the generation of the geometry of the specimen in ABAQUS™. The initial FE-model includes the material parameters, the boundary and loading conditions, and the initial uncracked mesh.
The simulation procedure consists of two parts: a pre-processing phase and a static finite element analysis.
In the pre-processing part, the initial FE-model is imported in FRANC3D and the crack geometry is inserted into the initial mesh to create a new finite element model for the cracked structure. The model is then partitioned into the global region and the local domain where the crack is expected to propagate.
The crack front is surrounded by several flexible concentric cylinders, referred to as "tube". The innermost tube layer is made up of "quarter-point" collapsed hexahedral elements, while the surrounding rings are based on 20-node brick elements [9],[11],[12] which encircle the collapsed elements at the crack front. The remaining volume of the domain is remeshed with quadratic tetrahedral elements. The mesh of the cracked domain is then merged with the hexahedral elements of the global region.
During the second phase of the model creation, the cracked model is imported in ABAQUS™ where it is possible to select the elastic-plastic stress-strain law of the material. Thereafter, the simulation itself takes place by means of the ABAQUS™ solver. Once the simulation is terminated, the results can be analysed. A dimensional assessment of the crack-tip-yielding permits to quantify the plasticity at the crack tip.

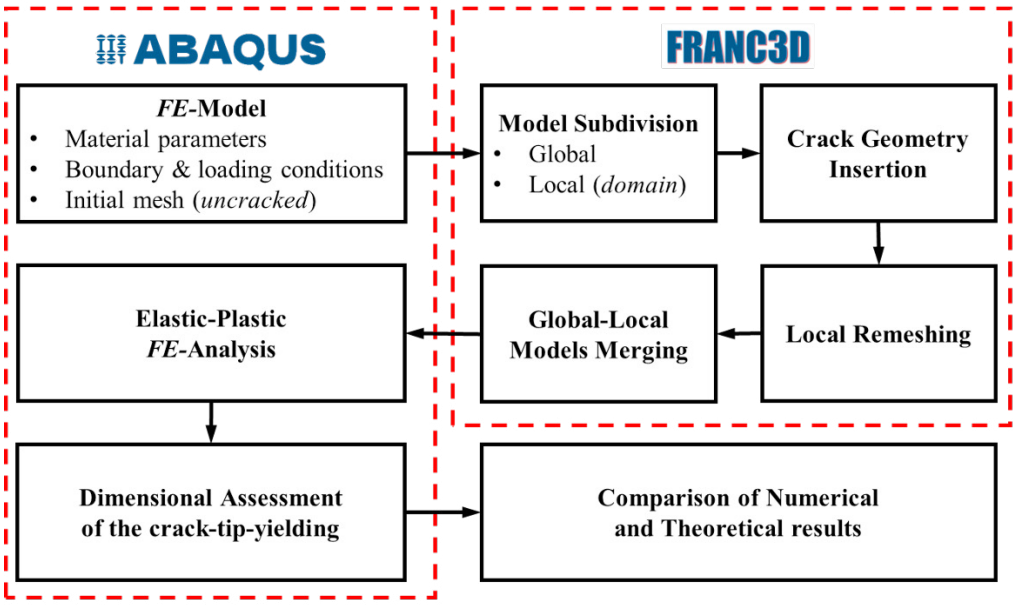

Fig. 3 Numerical simulation procedure with ABAQUS™ and FRANC3D.

4.2. Numerical Model

The numerical model was prepared in the ABAQUS™ environment and then the crack was inserted by means of FRANC3D code. In general, the mesh was kept coarse in the regions outside the propagation domain and very dense in the volume surrounding the crack surface. The size of elements surrounding the crack front was set to 20 μm, obtained as trade-off between convergence of results and computational burden. Fig. 4 shows the mesh of the specimen in the propagation increment right before the intersection of the crack front with the internal hole of the specimen (see also Fig. 1b). The global mesh is shown in grey whereas the tetrahedral elements of the domain are white coloured. The two close-up views show respectively the superficial mesh of propagation domain and the cross-section of the fine-meshed tube surrounding the crack front at the break-through point. The machinery clamps used in the tests to transfer the load were reproduced by clamping one extreme of the specimen and by loading in tension the other. For a more detailed description of the model, the reader is referred to [7].

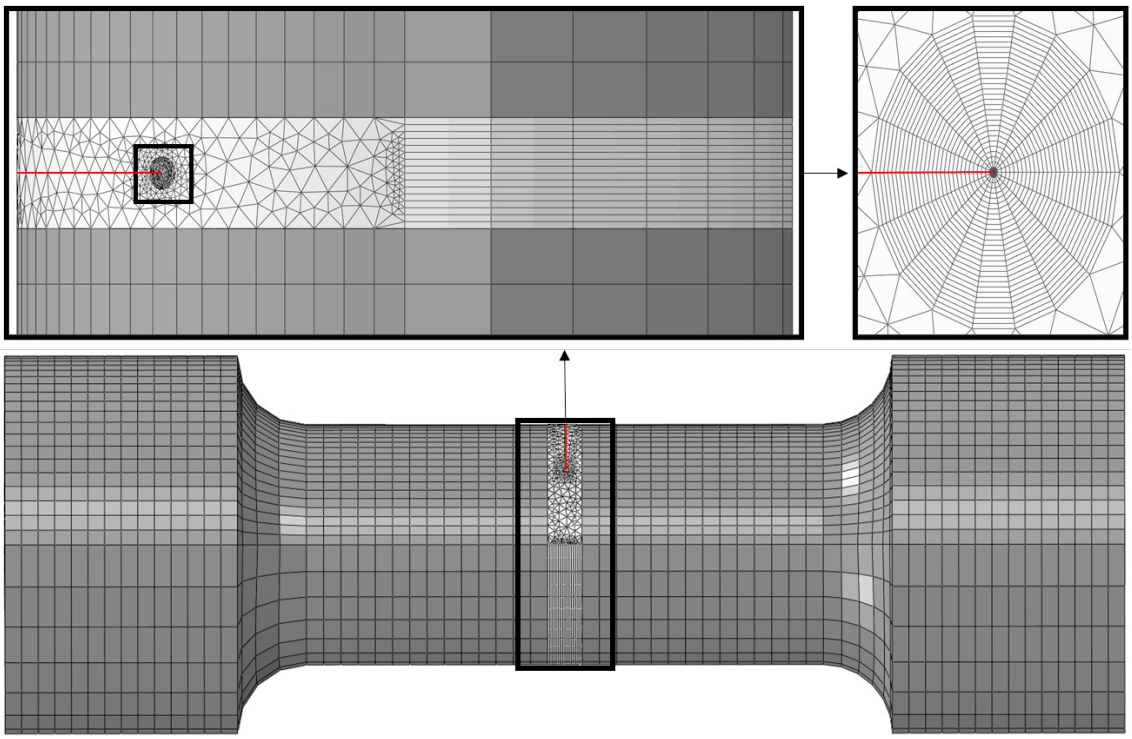

Fig. 4 FE-Model of the cracked specimen with a close-up on the domain and at the breakthrough point.

5. Plasticity zone comparison

The LEFM formulation of the SIF ($\sigma_{\theta=0} = \frac{K_I}{\sqrt{2\pi r}}$) assumes that for $r \to 0$ the stress at the crack tip grows indefinitely, independently from K_I. This is a consequence of the elasticity model of the material ($\sigma = E\epsilon$). In a real material, plastic deformations take place limiting the maximum value for the stress to the yield and causing a redistribution of

the stress. Under mode-I loading conditions, the theoretical shape of the plasticity zone can be expressed, through the Von Mises yielding criteria [13], as:

$$\begin{cases} r_P(\theta) = \frac{1}{4\pi}\left(\frac{K_I}{\sigma_y}\right)^2 \left(1 + \cos(\theta) + \frac{3}{2}\sin^2(\theta)\right) & \text{plane stress} \\ r_P(\theta) = \frac{1}{4\pi}\left(\frac{K_I}{\sigma_y}\right)^2 \left((1-2\nu)^2(1+\cos(\theta)) + \frac{3}{2}\sin^2(\theta)\right) & \text{plane strain} \end{cases} \quad (2)$$

These theoretical formulas do not rigorously predict the plastic zone extension and shape as they do not consider the redistribution of the stress due to yielding. FEM analyses are needed to estimate the exact plasticized zone around the crack front. The plastic zone size must be limited and engulfed within the singularity-dominated zone. Only if this condition is fulfilled it is possible to apply the LEFM formulation. In fact, if the plastic region is so large, relatively to some key dimensions, to engulf the singularity zone, the fracture cannot be *K*-controlled as the LEFM theory loses its validity. In laboratory testing, when evaluating the material fracture toughness, the following size requirements are usually adopted [14],[15]:

$$a, B, (W-a) \geq \frac{4}{\pi}\left(\frac{K_I}{\sigma_y}\right)^2 \approx 3.04\, mm \quad (3)$$

Where a represents the crack length, B the thickness and $(W-a)$ the dimension of the residual ligament ahead of the crack front. In this case study, with a K_I-SIF nearly constant along the crack front (Fig. 5) and on average equal to $800\ MPa\sqrt{mm}$ a residual ligament $(W-a) = 0.73\ mm$ does not fulfil the aforementioned requirement.
Fig. 5 shows the K_I-SIF distribution along the crack front approaching the hole (step 7), vs. a normalised abscissa (calculated as two times the relative node position along the front). To evaluate the validity of the LEFM approach used to replicate the testing conditions, the dimensions of the crack-tip-yielding have been evaluated. The plastic zone size obtained from the simulations has been compared with the theoretical formulas, to predict the crack-tip-yielding in the Dugdale formulation, in the plane of the crack ($\theta = 0$). In the case of analysis, the following theoretical formulas predict a crack-tip-yielding in the case of plane stress and plane strain respectively:

$$\begin{cases} r_P(\theta=0) = \frac{\pi}{8\alpha_{pss}}\left(\frac{K_I}{\sigma_y}\right)^2 = 0.779\, mm & \text{plane stress} \\ r_P(\theta=0) = \frac{\pi}{8\alpha_{psn}}\left(\frac{K_I}{\sigma_y}\right)^2 = 0.463\, mm & \text{plane strain} \end{cases} \quad (4)$$

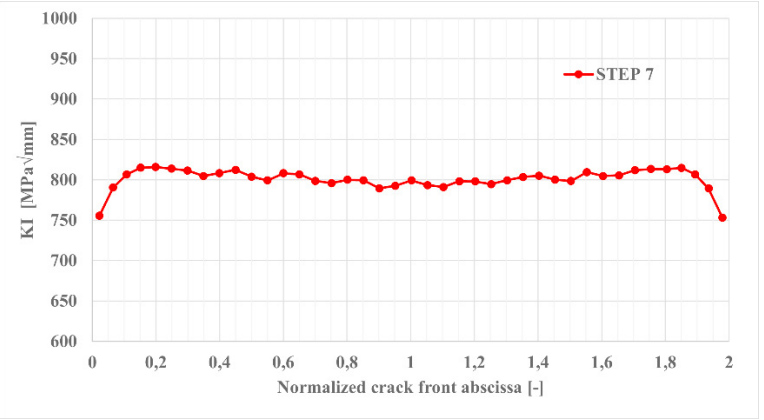

Fig. 5 K_I-SIF distribution for B95AT Al-alloy under tension.

The coefficient α in denominator was set to 1.2 and 2.1 in case of plane stress and plane strain, respectively. These values resulted in [16] as best fit with numerical data, in the plastic zone at $\theta = 0$.
The elastic-plastic analyses, performed with both B-L and R-O plasticity models, showed a significative crack-tip-yielding. With particular reference to R-O plasticity models, the numerical analyses showed: at the middle of the crack front, where a plain strain condition is supposed to exist, a $r_P(\theta = 0) \approx 0.37\ mm$; at the break-through point, where a plane stress condition is expected, a $r_P(\theta = 0) \approx 0.56\ mm$ was calculated.
In Fig. 6 the two zones of analysis are illustrated. The lower limit was set to about 80% σ_y; therefore, all the coloured areas have a stress level close to or above the yielding point. Fig. 6 (a) shows the size of the plastic region in the plane of the crack at the middle of the crack front. Fig. 6 (b) shows the dimension of the plasticised area at the break-through point for $\theta = 0$.

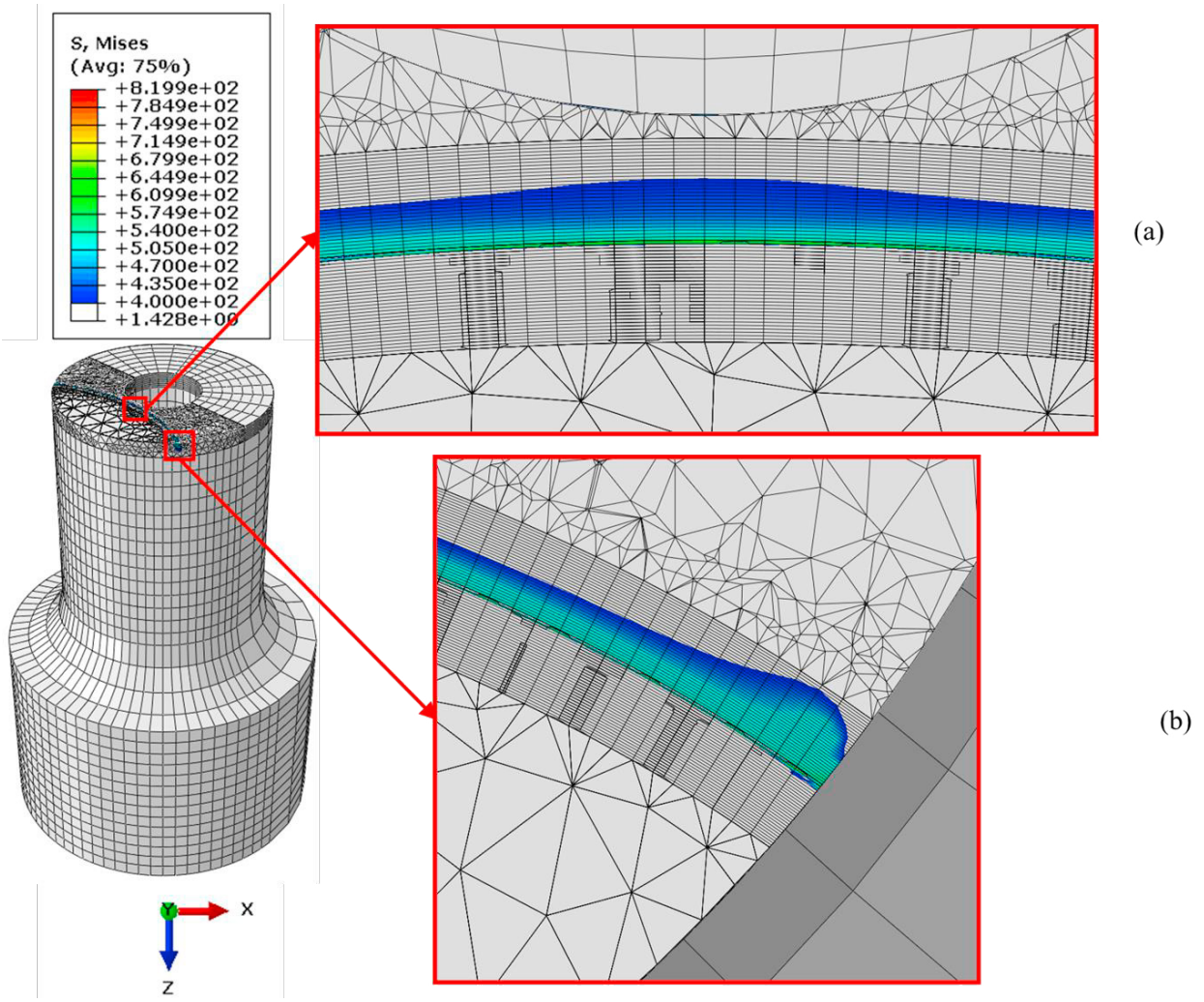

Fig. 6 (a) crack-tip-yielding; (b) plasticised area at the break-through point.

6. Discussion

The numerical analyses revealed a significative yielding ahead of the crack front. From Fig. 6 it is possible to notice that a non-negligible portion of the residual ligament ahead of the crack tip yielded. This is in contrast with the laboratory requirements for fracture tests. The comparison between the experimental and numerical results, shown in Fig. 7 and Fig. 8, exhibit an excellent agreement in terms of both crack growth (Fig. 7) and Crack Growth Rate (CGR) (Fig. 8), until a sufficient residual ligament exists ahead of the crack front. The crack configuration object of study, marked in green in Fig. 7 and Fig. 8, has a length of $a = 8.26\ mm$ and $b = 4.01$; in this configuration, a residual ligament of $0.73\ mm$ exits at middle of the crack front which turns out to be plasticized per half of its thickness. From the analysis of the aforementioned graphs, a clear mismatch between tests results and simulations is apparent as the crack front approaches the axial hole. Especially in terms of CGR, the numerical simulations begin to underestimate the crack growth in proximity of the intersection with the hole. The crack configuration analysed demonstrates that

the small residual ligament and the interaction between the crack and the hole generates an excessive plasticization ahead of the crack front that exceeds the limits of applicability of LEFM.

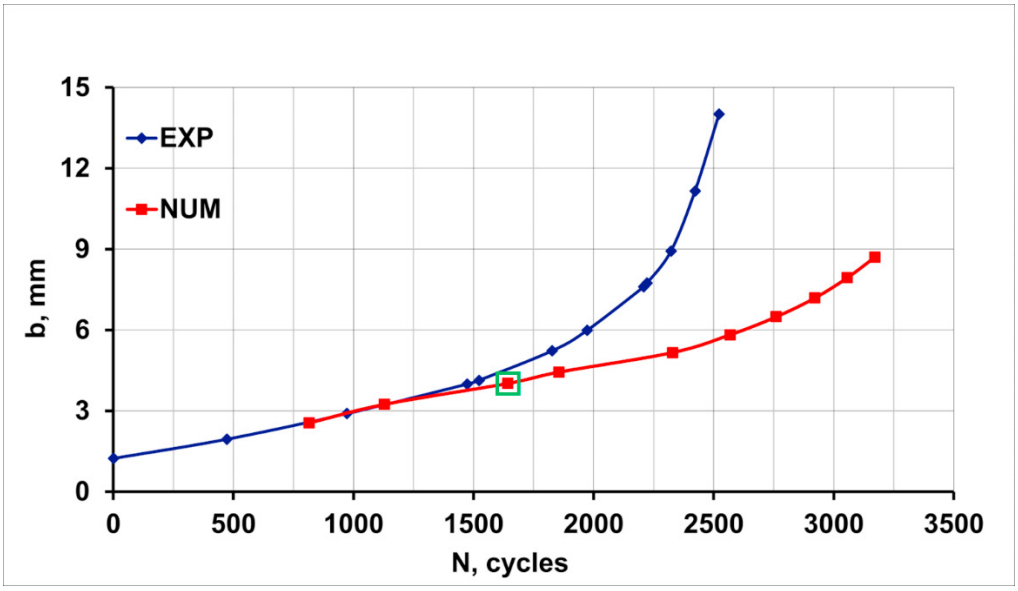

Fig. 7 Crack Length *b vs* Number of Cycles.

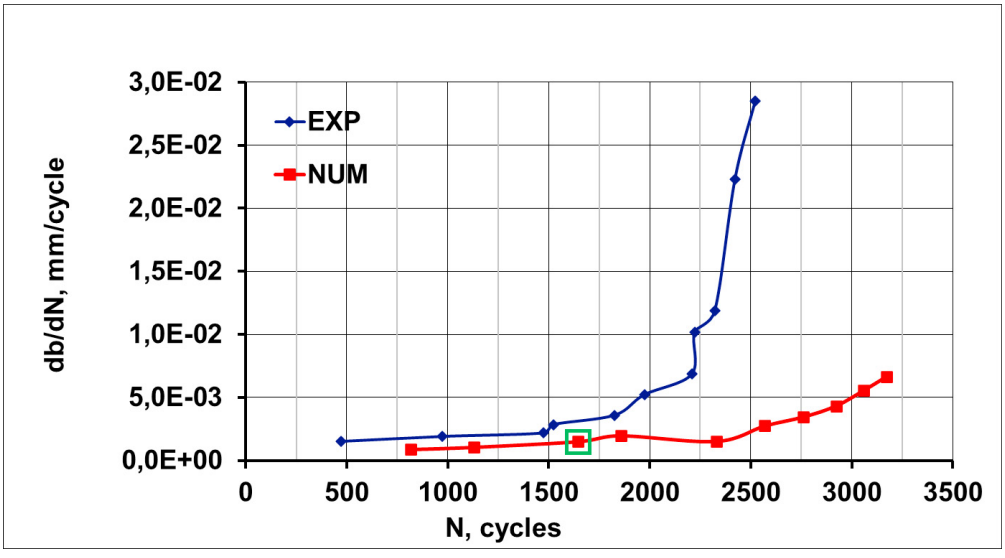

Fig. 8 Crack Growth Rate at breakthrough-point *vs* Number of Cycles.

7. Conclusion and Outlook

The aim of the study is to show that the LEFM theory is not always applicable to analyse real crack propagation in complex geometries. In fact, careful attention must be given to the limit of applicability of LEFM theory as not to exceed its boundaries. This study analyses the case study of a hollow cylindrical specimen with initial semielliptical surface crack, used to analyse fatigue crack growth under complex stress state, for which the LEFM limits are exceeded (due to insufficient residual ligament in comparison with crack tip plastic zone). The assessment of the crack-tip-yielding shows how the plastic zone size turns out to be comparable in size with the residual ligament and therefore the LEFM boundaries are exceeded. This outcome explains the misalignment found in [7] between the crack growth simulated by LEFM and the corresponding experimental results.

References

[1] Sehitoglu, Huseyin, K. Gall, and A. M. Garcia. "Recent advances in fatigue crack growth modeling." International journal of fracture 80 (1996): 165-192.
[2] She, Chongmin, and Wanlin Guo. "Three-dimensional stress concentrations at elliptic holes in elastic isotropic plates subjected to tensile stress." International Journal of Fatigue 29.2 (2007): 330-335.
[3] Ellyin, F., and J. Wu. "A numerical investigation on the effect of an overload on fatigue crack opening and closure behaviour." Fatigue & Fracture of Engineering Materials & Structures 22.10 (1999): 835-847.
[4] McClung, R. C. "Crack closure and plastic zone sizes in fatigue." Fatigue & fracture of engineering materials & structures 14.4 (1991): 455-468.
[5] Subramanya, H. Y., S. Viswanath, and R. Narasimhan. "A three-dimensional numerical study of mixed mode (I and II) crack tip fields in elastic–plastic solids." International Journal of Fracture 136 (2005): 167-185.
[6] González-Herrera, A., and J. Zapatero. "Influence of minimum element size to determine crack closure stress by the finite element method." Engineering fracture mechanics 72.3 (2005): 337-355.
[7] R. Yarullin, V. Shlyannikov, D. Amato, R. Citarella. "Mixed mode surface crack growth in aluminium alloys under complex stress state". Procedia Structural Integrity 2022; 39:364-378.
[8] Hill, H.N. : Determination of stress-strain relations from “offset” yield strength values, NACA TN No 927 , Feb. 1944
[9] FRANC3D V7.4 Reference.pdf. Available online: www.fracanalysis.com, accessed on 13th March 2023.
[10] ABAQUS manual. Available online: www.abaqus-docs.mit.edu, accessed on 13th March 2023.
[11] Barsoum R. On the use of isoparametric finite elements in linear fracture mechanics. Int J Numer Meth Engng. 1976;10: 25–37.
[12] Dhondt G. General behavior of collapsed 8-node 2-D and 20-node 3-D isoparametric elements. Int J Numer Meth Engng, 1993;36: 1223–1243.
[13] Anderson, Ted L. Fracture mechanics: fundamentals and applications. CRC press, 2017.
[14] E 399-90, “Standard Test Method for Plane-Strain Fracture Toughness of Metallic Materials.” American Society for Testing and Materials, Philadelphia, PA, 1990.
[15] Brown, W.F., Jr. and Srawley, J.E., Plane Strain Crack Toughness Testing of High Strength Metallic Materials. ASTM STP 410, American Society for Testing and Materials, Philadelphia, PA, 1966.
[16] Newman Jr, J. C., E. L. Anagnostou, and D. Rusk. "Fatigue and crack-growth analyses on 7075-T651 aluminum alloy coupons under constant and variable-amplitude loading." International Journal of Fatigue 62 (2014): 133-143.